Article

High-Resolution Photoelectron Spectroscopy of Vibrationally Excited Vinoxide Anions

Published as part of The Journal of Physical Chemistry A virtual special issue "Honoring Michael R. Berman".

Jascha A. Lau,[⊥] Martin DeWitt,[⊥] Mark A. Boyer, Mark C. Babin, Tonia Solomis, Max Grellmann, Knut R. Asmis, Anne B. McCoy, and Daniel M. Neumark*

ACCESS | Metrics & More | Article Recommendations | Supporting Information

ABSTRACT: High-resolution photoelectron spectra of vibrationally pre-excited vinoxide anions (CH_2CHO^-) are reported using the recently developed IR-cryo-SEVI technique. This method is combined with a newly developed implementation of vibrational perturbation theory that can readily identify relevant anharmonic couplings among nearly degenerate vibrational states. IR-cryo-SEVI spectra are obtained by resonant infrared excitation of vinoxide anions via the fundamental C−O (ν_4, 1566 cm^{-1}) or isolated C−H (ν_3, 2540 cm^{-1}) stretching vibrations prior to photodetachment. Excitation of the ν_4 mode leads to a well-resolved photoelectron spectrum that is in excellent agreement with a harmonic Franck−Condon simulation. Excitation of the higher-energy ν_3 mode results in a more complicated

spectrum that requires consideration of the calculated anharmonic resonances in both the anion and the neutral. From this analysis, information about the zeroth-order states that contribute to the nominal ν_3 wave function in the anion is obtained. In the neutral, we observe anharmonic splitting of the ν_3 fundamental into a polyad feature with peaks at 2737(22), 2 835(18), and 2910(12) cm^{-1}, for which only the center frequency has been previously reported. Overall, 9 of the 12 fundamental frequencies of the vinoxy radical are extracted from the IR-cryo-SEVI and ground-state cryo-SEVI spectra, most of which are consistent with previous measurements. However, we provide a new estimate of the ν_5 (CH$_2$ scissoring) fundamental frequency at 1395(11) cm^{-1} and attribute the discrepancy with previously reported values to a Fermi resonance with the $2\nu_{11}$ overtone (CH$_2$ wagging).
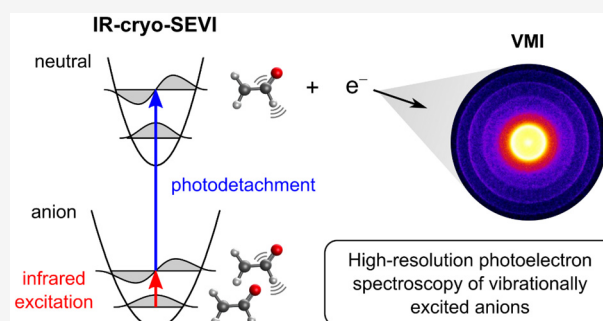
1. INTRODUCTION

Anion photoelectron spectroscopy (PES) is a versatile technique that has been used to probe the spectroscopy and energetics of reactive free radicals,[1,2] a wide range of clusters,[3−6] and transition states for unimolecular and bimolecular reactions.[7−9] It enables precise measurements of electron affinities for atomic and molecular species[10] and is capable of probing electronic and vibrational structure in the ground and excited electronic states of neutral species that are accessible via photodetachment. The selection rules for PES are more relaxed compared to conventional bound−bound electronic absorption spectroscopy due to the angular momentum transferred to the photoelectron. Moreover, photodetachment does not require resonant excitation as a mismatch between the photon and transition energy can be compensated by the kinetic energy of the outgoing electron.[9,11,12] Our laboratory has devoted considerable effort to improving the energy resolution of anion PES through the technique of cryo-SEVI (slow photoelectron velocity-map imaging of cryogenically cooled anions), which yields vibrationally resolved spectra with a resolution down to ~1 cm^{-1}.[13−15] At this higher resolution, one can resolve

progressions in multiple vibrational modes that could not be seen in more conventional PES experiments.[16,17] Here, we present a significant extension of cryo-SEVI by exploring the effects of vibrational pre-excitation of a polyatomic anion, the vinoxide anion (CH_2CHO^-), prior to photodetachment. Our experiment complements work on neutral species that has explored the effects of IR excitation on high-resolution zero-electron kinetic energy spectra.[18,19]

The motivation for vibrational pre-excitation is evident from Figure 1. In anion PES, the intensities of transitions from the anion ground state to vibrationally excited neutral levels are typically governed by Franck−Condon (FC) factors, in which case one only observes progressions in those totally symmetric vibrational modes for which there is a normal coordinate
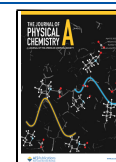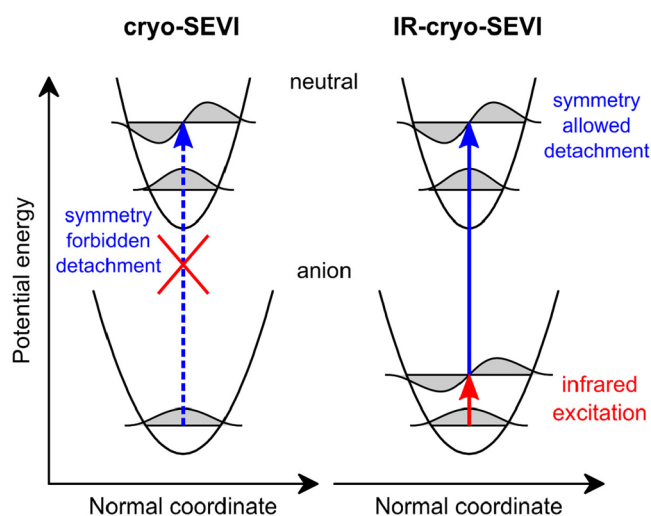
Figure 1. Schematic illustration of how infrared excitation of a non-totally symmetric anion vibration results in new vibrational transitions becoming accessible via photodetachment. Red arrows indicate IR excitation in the anion, and blue arrows indicate photodetachment.

displacement upon photodetachment. There is no such displacement for symmetry reasons in non-totally symmetric modes, while for totally symmetric modes comprising C−H, O−H, and N−H stretches, the changes in bond lengths are generally very small.[20−22] Hence, the situation on the left side of Figure 1 holds; the transition strength from the anion ground state to the $v = 1$ level of a non-totally symmetric mode or a mode in which there is no normal coordinate displacement is either zero by symmetry or negligibly small. However, excitation of the $v = 1$ level of one of these modes in the anion results in a fully FC-allowed transition to the neutral $v = 1$ level, as shown on the right side of Figure 1, leading to new features in the photoelectron spectrum.

We recently reported cryo-SEVI spectra of OH⁻, in which an infrared (IR) laser excited OH⁻ from the $(v = 0, J = 0)$ ground state to the $(v = 1, J = 1)$ level before photodetachment by a visible laser pulse.[23] This experiment was the first demonstration of cryo-SEVI in combination with prior infrared excitation (IR-cryo-SEVI), but the application of this approach to studies of polyatomic molecules has not yet been reported. There are several fundamental challenges to such an experiment. First, vibrational frequencies in polyatomic anions are generally less well-characterized compared to their neutral counterparts. Second, the rotational level structure of a polyatomic molecule is denser compared to OH⁻. As a result, one does not expect to be able to excite individual rotational transitions with the 3.7 cm⁻¹ excitation laser bandwidth used in the IR-cryo-SEVI experiment. Finally, anharmonic coupling in the anion can result in a vibrationally excited state that shows contributions from several zeroth-order states, each of which has a distinct contribution to the photoelectron spectrum. This may lead to a more complex spectrum than implied by Figure 1. The effects of anharmonic coupling in the electronic ground states of molecules have been investigated by a variety of frequency-resolved techniques, including high-resolution IR absorption spectroscopy, overtone pumping, dispersed IR fluorescence, stimulated emission pumping and other double-resonance techniques.[24−26] Depending on the extent of anharmonic coupling, IR-cryo-SEVI could provide a new approach to simultaneously obtain state-specific information on anharmonic

coupling in the ground electronic states of both the anion and the neutral.

In the presence of anharmonic coupling, assignment of IR-cryo-SEVI spectra requires extensions to existing theoretical methods, as one observes a transition from a vibrationally excited state in the anion to a vibrationally excited state in the neutral. Therefore, the theoretical treatment requires the evaluation of wave functions and energies for the vibrational states of both the anion and the neutral, as well as transition intensities between these states. In the simplest approach, one would model the vibrations as harmonic oscillators. Existing software packages[27,28] can then be used to evaluate the FC overlap between the harmonic wave functions in the anion and neutral. Including the effects of state-mixing among the vibrational states, however, requires methods beyond the harmonic approximation, done here within the framework of nearly degenerate vibrational perturbation theory (VPT).[29−31]

The vinoxide anion (CH₂CHO⁻) is an appropriate system to explore with IR-cryo-SEVI owing to its well-studied photo-detachment spectrum measured in several laboratories,[32−38] including a high-resolution SEVI study from our group.[38] The neutral vinoxy radical is relevant to combustion chemistry, appearing as an intermediate in the oxidation of terminal alkenes,[39] and its dissociation dynamics have been studied in detail.[40−43] The geometry of the vinoxy radical reflects contributions from two planar resonance structures. The dominant contribution to its $\tilde{X}^2A''$ ground state comes from a formyl methyl structure (CH₂CH=O), with the free electron on the methylene carbon, rather than the vinoxy structure (CH₂=CHO) implied by its name, where the unpaired electron would be located on the oxygen atom. This structure was recognized early on in matrix IR absorption studies[44] and is consistent with high-level ab initio calculations[45] as well as the spin density on the methylene carbon obtained from microwave spectra.[46,47] The vinoxide anion in its $\tilde{X}^1A'$ ground state has a similar geometry to the radical with slightly longer C−O and slightly shorter C−C bond lengths based on calculations, more resembling the vinoxy structure.[36,38,48]

Several spectroscopic techniques have been applied to study the vibrational structure of the vinoxy radical, but the determination of fundamental frequencies for its C−H stretching vibrations has been surprisingly challenging. IR absorption studies of vinoxy radicals isolated in an Ar matrix[44] could not probe any of the C−H stretch fundamental frequencies $(\nu_1 - \nu_3)$ due to technical limitations. The vibrational structure of the ground state was further investigated in the gas phase by multiple laser-induced fluorescence (LIF) studies based on the $\tilde{B}^2A'' \rightarrow \tilde{X}^2A''$ electronic transition.[49−53] Early LIF studies[49,50] focused mainly on the C−O stretching (ν_4), C−C stretching (ν_7), and C−C−O (ν_9) bending vibrations, which show the highest FC activity owing to the different geometry of the C−C−O backbone in the ground and excited electronic states.[40,54] Reanalysis of this LIF data[51] and additional LIF measurements[52,53] enabled assignments of the $\nu_4 - \nu_{12}$ modes. However, the C−H stretch fundamentals $(\nu_1 - \nu_3)$ are not FC-active in those LIF experiments and have not been observed. To date, only a single measurement of the ν_3 fundamental based on multipass IR laser absorption spectroscopy in a supersonic jet has been reported, placing the band origin at 2827.913 cm⁻¹.[55]

The vinoxide anion has also been the focus of several spectroscopic investigations. Early reports of its photodetachment spectra yielded an estimate of the electron affinity of the

vinoxy radical but showed little vibrational structure.[32,34] In addition, a dipole-bound anion state exists only a few cm^{-1} below the detachment threshold.[33,35] Photodetachment spectra encompassing the $\tilde{X}^2A''$ and $\tilde{A}^2A'$ states of the neutral were reported by Continetti and co-workers, showing some vibrationally resolved features.[36,37] SEVI spectra have been reported for vinoxide[38] and two of its derivatives.[56,57] The SEVI spectra by Yacovitch et al.[38] resolved vibrational levels within the $\tilde{X}^2A''$ and $\tilde{A}^2A'$ states of the vinoxy radical and provided a precise determination of its electron affinity (14 719(9) cm^{-1}). The ground-state spectrum showed extended activity in the neutral ν_4, ν_7, and ν_9 modes. This work was done prior to the incorporation of cryogenic cooling into the instrument, and hot band transitions due to incomplete cooling complicated the assignment for low-intensity lines.

In this work, we report cryo-SEVI spectra of vinoxide selectively prepared in its vibrational ground state as well as in vibrationally excited states by IR laser excitation of the ν_4 (C−O stretching) and ν_3 (C−H stretching) fundamentals at 1570 and 2546 cm^{-1}, respectively, prior to photodetachment. We show that the ν_4 vibration in the anion is weakly coupled to other vibrations, whereas excitation of the ν_3 fundamental followed by photodetachment shows evidence for strong anharmonic coupling within the anion and the neutral, leading to complex spectra that require analysis beyond harmonic FC simulations. Assignment of all spectra presented here allows us to extract fundamental vibrational frequencies of the vinoxy radical for all vibrational modes except for the two higher-frequency C−H stretching vibrations (ν_1 and ν_2) and the isolated C−H wagging vibration (ν_{10}). We discuss discrepancies between our observations and previous observations for the ν_3 and ν_5 fundamentals as well as state-specific information on anharmonic coupling in both the anion and the neutral extracted from the ν_3 IR-cryo-SEVI spectra. Finally, we consider the potential of using IR-cryo-SEVI in combination with our implementation of VPT to investigate other polyatomic systems.

2. EXPERIMENTAL METHODS

The apparatus for high-resolution photoelectron spectroscopy based on anion cryo-SEVI has been described in detail elsewhere.[13−15,23] To make vinoxide anions, helium gas mixed with trace amounts of acetaldehyde and N$_2$O is expanded through a pulsed Even−Lavie valve coupled to a filament ionizer.[58] Dissociative electron attachment to N$_2$O produces O$^-$ ions that abstract a methyl proton from acetaldehyde to form C$_2$H$_3$O$^-$. The anions pass through a skimmer into a guiding radiofrequency (RF) hexapole and then through an RF quadrupole filter for initial mass selection. The mass-selected ions enter a linear octupole ion trap held at 5 K, in which they are stored for ∼40 ms while being cooled through collisions with a H$_2$/He buffer gas mixture (20%/80%).[14] The cooled anions are extracted into an orthogonal Wiley−McLaren time-of-flight mass spectrometer.[59] At the end of a ∼2 m long flight path, ions of the desired mass are photodetached by an appropriately timed laser pulse within a 7-plate velocity-map imaging (VMI) lens assembly designed to optimize resolution for slow electrons.[15] A set of gated deflector plates only allows ions of approximately the correct mass to enter the VMI region.

For photodetachment, the output of a dye laser (Radiant Dyes NarrowScan) pumped by the second harmonic of a nanosecond Nd:YAG laser (Spectra-Physics Quanta-Ray PRO-290), operating at 20 Hz, is used. The detached photoelectrons are mapped onto a position-sensitive imaging detector comprising two chevron-stacked microchannel plates and a phosphor screen. Images are acquired at a repetition rate of 20 Hz with a charge-coupled device (CCD) camera (768 × 768 pixels). Individual electron spots are event-counted and binned onto a 1024 × 1024 grid using the hybrid gradient-center of mass (HGCM) centroiding algorithm introduced in ref 60.

The addition of an OPO/OPA IR laser system (LaserVision, 3.7 cm^{-1} bandwidth), pumped by a Nd:YAG laser (Continuum SureLite SLIII-EX), for IR-cryo-SEVI has been previously described.[23] A schematic of the optical setup, including some additional details, can be found in Figure S1. The OPO/OPA is operated at half the repetition rate of the detachment laser (10 Hz) to enable a direct, shot-to-shot comparison between photodetachment with (IR-on) and without (IR-off) IR pre-excitation. IR wavelengths are calculated from the near-IR frequency of the signal in the OPO stage determined with a wavemeter (Coherent WaveMaster). To excite the ν_3 vibration of vinoxide at 2546 ± 1 cm^{-1}, we directly use the idler output of the OPA at a typical pulse energy of ∼2.0 mJ. To excite the ν_4 vibration at 1570 ± 2 cm^{-1}, we add an additional difference frequency generation (DFG) stage to mix the OPA signal and idler in an AgGaSe$_2$ crystal, resulting in mid-IR radiation with a typical pulse energy of 1.0−1.6 mJ. For the detachment laser, pulse energies of 2−4.5 mJ were used.

The counterpropagating IR and detachment laser beams are focused and overlapped in the VMI region of the vacuum chamber using CaF$_2$ lenses with focal lengths of 500 and 1000 mm, respectively. The IR laser focus diameter is estimated as 0.5 and 0.9 mm at 2550 and 1550 cm^{-1}, respectively, ensuring that the IR excitation region is larger than that of the detachment laser for which the estimated focus diameter is <0.2 mm. Both laser pulses are also temporally overlapped on a photodiode outside the vacuum chamber using the visible dye laser light and near-IR light from the OPO/OPA; this condition led to the strongest IR-induced signals in our experiment.

Photoelectron velocity-map images are processed using the maximum entropy velocity Legendre reconstruction (MEVEL-ER) algorithm[61] to obtain reconstructed radial and angular distributions. The radial distribution of the spectrum is related to the electron kinetic energy (eKE) through a calibration based on the well-known photodetachment transitions for atomic O$^-$ at various photon energies.[62] The electron binding energy (eBE) is obtained from the eKE and the photon energy, $h\nu$, by eBE = $h\nu$ − eKE. High-resolution scans are composed of individual scans at different photon energies, close to the transitions of interest, to benefit from the improved resolution of our setup for slow photoelectrons. The intensities of these scans are scaled to match a lower-resolution overview spectrum obtained at a photon energy that is sufficiently high to access most (if not all) of the vibrational bands of interest. To account for the relatively low signals that appear for new features after IR pre-excitation, 4−5 images were typically acquired for the same photon energy under comparable conditions and individually reconstructed. The resulting photoelectron spectra were then added.

From the reconstructed angular distribution, anisotropy parameters, β, can be obtained that contribute to the differential photodetachment cross section according to eq 1 for linearly polarized light.[63,64]

$$\frac{d\sigma}{d\Omega} = \frac{\sigma_{\text{total}}}{4\pi}(1 + \beta P_2(\cos\theta)) \tag{1}$$

Here, σ_{total} is the total photodetachment cross section, $P_2(x)$ is a second-order Legendre polynomial, and θ describes the angle between the direction of the detached electron and the polarization vector of the laser light. The anisotropy parameter lies between -1 and $+2$ for perpendicular and parallel detachment, respectively. Its dependence on eKE gives information on the electronic state and molecular orbital from which photodetachment occurs.

3. COMPUTATIONAL DETAILS

3.1. Generalized Vibrational Perturbation Theory Calculations. As will be seen later, excitation of the ν_3 mode of the anion leads to photoelectron spectra that cannot be described by simple harmonic analysis. Analysis of these spectra requires a way to account for anharmonic coupling in both anion and neutral. To aid in the interpretation of these effects, vibrational perturbation theory (VPT)[30,31,65] calculations were performed using PyVPTn,[66,67] which provides an implementation of VPT in a matrix representation. All VPT calculations were performed using normal mode coordinates that are constructed from linear combinations of valence coordinates. The valence coordinates used to construct the normal modes and their values at the minimum energy structures are provided in Table S1. The normal modes of the anion and neutral are illustrated in Figures S2 and S3. The requisite quartic expansion of the potential in these coordinates was obtained at the B2PLYP-D3/aug-cc-pVTZ level of theory and basis by numerically evaluating the first and second derivatives of the Hessian with respect to each of the $3N$-6 normal modes, as implemented in Gaussian 16.[68] The choice to use this level of theory is based on its effectiveness for studies of similar organic radicals.[69]

Critical to these calculations is the ability to identify nearly degenerate states.[29,31,70−72] In vibrational perturbation theory without consideration of resonances, corrections to the zeroth-order states and energies are obtained as vectors of expansion coefficients in the basis composed of the zeroth-order states. When resonances are present, this procedure must be modified. For the calculations performed in this study, a resonance between states n and m was identified if the expansion coefficient from state m for the corrections to state n at any order of correction was >0.3 or vice versa. We also introduce the requirement that, for a given state of interest, the set of states resonant with this state spans an energy range of no more than 500 cm^{-1}. These criteria were found to be effective in a previous study.[71] This results in a resonant space consisting of three states for the ν_3 state in H$_2$CCHO$^-$ and 31 states that make up the resonant space for the corresponding state in H$_2$CCHO. Additionally, a resonance between the ν_3 state and the $\nu_4 + \nu_8$ state was introduced to the set of nearly degenerate states in the anion, resulting in a final resonant space consisting of four states. This resonance is not identified through the resonance criterion introduced earlier, which is based on the ratio of the coupling matrix element involving this pair of states to the difference between their harmonic frequencies; their harmonic frequencies differ by ∼140 cm^{-1}, while the matrix element is only ∼7 cm^{-1}. However, the difference between the anharmonic frequencies of these two states reduces the energy difference to only ∼10 cm^{-1}, leading to a strong resonance interaction between these two states once diagonal anharmonicities are considered.

Once the resonances are identified, a second VPT calculation is performed in which all nearly degenerate states are projected out of the basis. This calculation provides the deperturbed energies of these nearly degenerate states as well as the matrix

elements of the Hamiltonian in the basis of these deperturbed states. The Hamiltonian, expressed in the basis of deperturbed states, is then diagonalized to obtain the anharmonically coupled vibrational wave functions and corresponding frequencies. This corresponds to a 4×4 matrix for the ν_3 state in H$_2$CCHO$^-$ and a 31×31 matrix for H$_2$CCHO. Additional details of this approach for identifying resonances and the evaluation of the Hamiltonian matrix are described elsewhere.[71] The calculated coupling matrices and corresponding coefficients used to express the vibrational wave functions in the basis of deperturbed states can be found in the Supporting Information.

Finally, some of the diagonal elements of these coupling matrices in the basis of nearly degenerate states are shifted, as detailed in Section S1.1 (supported by Figures S4 and S5). For the neutral, this includes a shift of -50 cm^{-1} for the harmonic ν_4 frequency to match the calculated ν_4 fundamental frequency with the experimental value, affecting the deperturbed frequencies of all modes that involve ν_4 excitation in a similar manner. For the anion, the deperturbed frequencies of the $\nu_4 + \nu_8$ and $2\nu_6$ states were directly shifted by about -20 and $+40$ cm^{-1}, respectively, motivated by observations in the photodetachment spectrum following ν_3 excitation. This is necessary as the extent of the couplings between the states can be sensitive to small shifts in their energies and induce variations from the experimentally observed frequencies and spectra. A similar strategy was employed in a recent study of the vibrational spectra of complexes formed between halide ions and HOCl.[73]

3.2. Calculation of Anharmonic Franck−Condon Spectra. Franck−Condon (FC) spectra, including Duschinsky rotations between all modes,[74] were simulated using ezFCF 1.2 within the harmonic approximation.[27,28] Those spectra were calculated for the vibrational ground state and selected vibrationally excited states of the anion. FC spectra of vibrationally excited anion states with up to three quanta were obtained by simulating a full spectrum at 300 K and extracting the FC factors for the transitions of interest. Unless otherwise stated, eBE values were calculated based on the anharmonic anion and neutral frequencies from the B2PLYP-D3/aug-cc-pVTZ calculations. Note, however, that the corresponding FC spectra still rely on FC factors calculated with harmonic wave functions. All FC calculations were performed using Cartesian coordinates for the minimum energy structures (Table S2) and normal coordinates.

For simulation of the ν_3 IR-cryo-SEVI spectra, a different approach is used to account for anharmonic corrections to peak positions (see Section S1.2) and anharmonic intensities (described in the following). There, anion and neutral wave functions are considered, which each contain contributions from various anharmonically coupled zeroth-order states. For the anion, the vibrationally excited state is described by

$$|\chi_i''\rangle = \sum_j c_j'' |\phi_j''\rangle \tag{2}$$

where the $|\phi_j''\rangle$ comprise the set of states that are nearly degenerate with the state of interest, here the ν_3 mode in the anion. This set of states is identified in the VPT2 calculation (see Section 3.1), and the elements of the Hamiltonian matrix, expressed in this basis, are obtained from the deperturbed VPT2 calculation. The mixing coefficients c_j'' are obtained from diagonalization of this Hamiltonian matrix. Equivalently, we define the anharmonic vibrational wave function in the neutral as

$$|\chi'_f\rangle = \sum_k c'_k |\phi'_k\rangle \tag{3}$$

Here, c'_k and $|\phi'_k\rangle$ provide the mixing coefficients and zeroth-order states within the resonant space of the final vibrational state in the neutral. The anharmonic FC factors, which are the square of the $\langle\chi'_f|\chi''_i\rangle$ matrix elements, are thus given by eq 4. The summation runs over all zeroth-order states in the resonant space of the anion (index j) and the neutral (index k).

$$|\langle\chi'_f|\chi''_i\rangle|^2 = \left|\sum_{j,k} c'_k c''_j \langle\phi'_k|\phi''_j\rangle\right|^2 \tag{4}$$

For the evaluation of these FC factors, we approximate the actual zeroth-order state wave functions $|\phi''_j\rangle$ and $|\phi'_k\rangle$, obtained from the deperturbed VPT2 calculations, by the corresponding harmonic wave functions $|\phi''_{h,j}\rangle$ and $|\phi'_{h,k}\rangle$, which will be referred to as zeroth-order states in the following:

$$I_{i,f} = \left|\sum_{j,k} c'_k c''_j \langle\phi'_{h,k}|\phi''_{h,j}\rangle\right|^2 \tag{5}$$

The quantity $I_{i,f}$ provides an approximate way to evaluate anharmonic FC factors that include state mixing based on harmonic zeroth-order states, and it is used for the anharmonic FC simulations shown in the present work. The harmonic FC overlaps, $\langle\phi'_{h,k}|\phi''_{h,j}\rangle$, are again calculated with ezFCF. Note that eq 5 is expected to provide a good approximation to eq 4 because $|\phi''_j\rangle$ and $|\phi'_k\rangle$ result from deperturbed VPT calculations, making the contributions from other states to these wave functions small compared to the leading term in the expansion. This approach to calculating anharmonic FCFs (including Duschinsky rotations) is similar to the ones described in refs 75 and 76 but relies on anharmonic wave functions obtained from vibrational perturbation theory instead of variational anharmonic calculations.

For the special case that the neutral wave function can be represented by a single zeroth-order state, $|\chi'_f\rangle \approx |\phi'_{h,f}\rangle$, eq 5 reduces to

$$I_{i,f}^{(uc)} = \left|\sum_j c''_j \langle\phi'_{h,f}|\phi''_{h,j}\rangle\right|^2 \tag{6}$$

4. RESULTS

4.1. Photoelectron Spectra of Ground-State and Vibrationally Excited Vinoxide.
4.1.1. Photoelectron Spectra of Ground-State Vinoxide. The cryo-SEVI spectrum of vinoxide in its vibrational ground state is presented in Figure 2, showing an overview spectrum (blue trace) and high-resolution scans (black traces). Peak positions obtained from Gaussian fits to the high-resolution spectra are listed in Table 1. Note that these spectra are collected at the same time as the data for the vibrationally excited ions.

The cryo-SEVI spectrum is dominated by a few intense features, labeled "A*n*", that agree well with the main features observed in previous SEVI measurements when using the overview spectrum in Figure 2 for comparison.[38] Some features in the spectrum consist of two peaks, showing either a shoulder at low eBE (A4/5 and A8/9) or a resolved doublet in the high-resolution spectra (A6/7), not previously resolved in ref 38. A1 is readily assigned to the vibrational origin. As also reported in ref 38, the intense peaks A2, A3, and A6 clearly form a
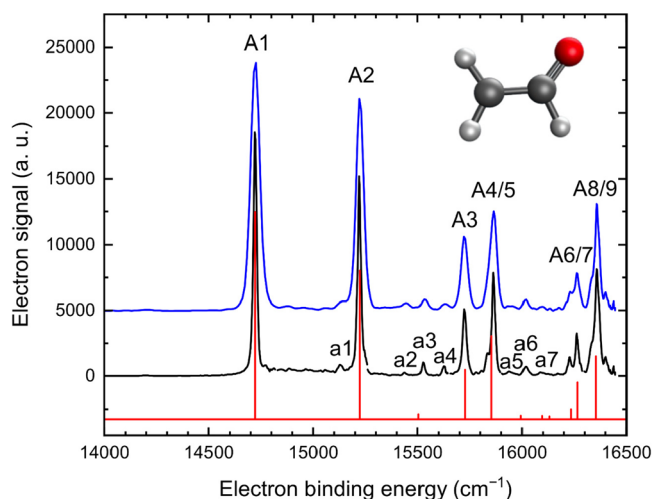

Figure 2. Overview photoelectron spectrum of the vinoxide anion taken at a detachment photon energy of 16 446 cm^{-1} without IR excitation (top trace, blue curve). Corresponding high-resolution spectra taken at several lower photon energies and scaled to reflect the intensities in the overview spectrum (center trace, black curves). Harmonic Franck–Condon simulation for detachment from the vibrational ground state of the anion (bottom trace, red curve) (see Section 3.2 for details).

Table 1. Electron Binding Energies (eBEs) and Assignments for the Ground-State Cryo-SEVI Spectrum

peak	eBE^a (cm^{-1})	assignment	shift to 0_0^0	shift to 9_0^1
A1	14 721(8)	0_0^0	0	
a1	15 129(10)	12_0^1	408	
A2	15 220(8)	9_0^1	499	0
a2	15 438(6)	11_0^1	717	218
a3	15 527(7)	12_0^2	805	306
a4	15 625(8)	$9_0^1 12_0^1$	904	405
A3	15 724(10)	9_0^2	1003	504
A4	15 835(9)	$11_0^1 12_0^{1b}$	1114	615
A5	15 864(8)	7_0^1	1143	644
a5	15 941(17)	12_0^3	1220	721
a6	16 018(11)	$9_0^1 12_0^2$	1297	798
a7	16 094(15)	6_0^1	1373	874
A6	16 228(8)	9_0^3	1507	1008
A7	16 263(9)	4_0^1	1542	1043
A8	16 330(8)	$9_0^1 11_0^1 12_0^{1b}$	1609	1110
A9	16 360(11)	$7_0^1 9_0^1$	1639	1140

^{a}Electron binding energies are determined from Gaussian fits to the highest-resolution scan for that peak and the uncertainties in parentheses are estimated as 1σ, based on the widths of the Gaussian fits. ^{b}Assignment based on the sum of the ν_{11} and ν_{12} fundamentals. The resulting estimate of 1114(9) cm^{-1} for the $\nu_{11} + \nu_{12}$ combination also agrees well with the assignment of Thomas et al.[48]

progression in the ν_9 mode with spacing ~500 cm^{-1}. Other assignments can be found in Table 1 and will be discussed in more detail in Section 4.2. In addition, the main features all share the same anisotropy parameter β as a function of eKE (see Figure S6). An additional set of much less intense features is observed and labeled "a*n*". For those weak features, another progression (a1, a3, a5) with spacing ~400 cm^{-1} is identified.

4.1.2. Pre-excitation of the C–O Stretching Mode (ν_4 IR-cryo-SEVI Spectrum). Figure 3a shows an IR-off velocity-map image, while Figure 3b shows the corresponding IR-on image with the IR laser tuned to the C–O stretching (ν_4) fundamental
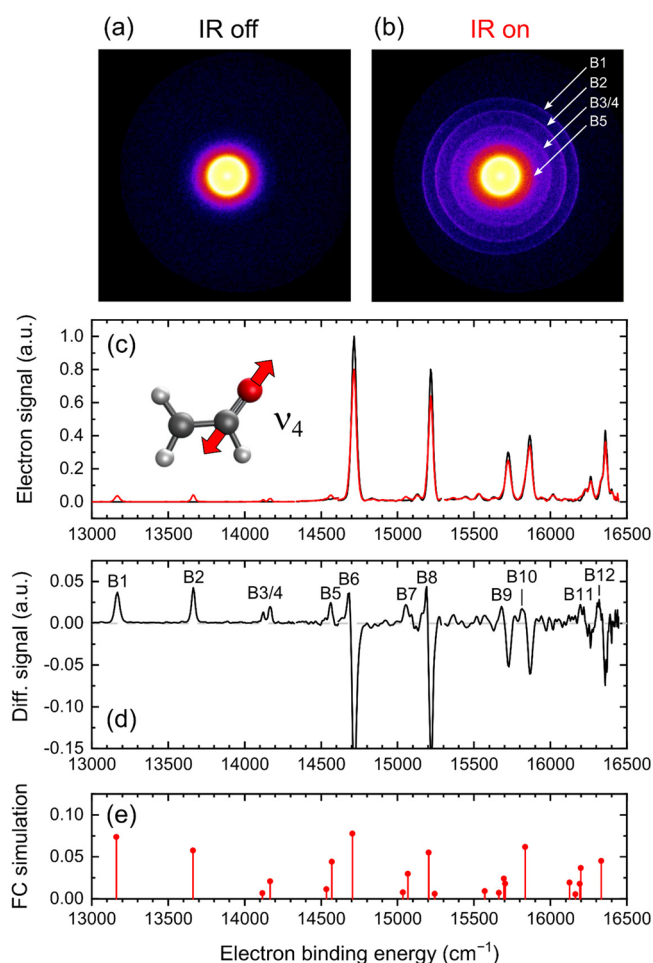
Figure 3. (a) Accumulated velocity-map image obtained from experimental cycles where the IR laser is not firing (IR-off) at a photodetachment energy of 14 810 cm^{-1}. (b) Simultaneously acquired image for the cycles where the IR laser vibrationally excited the vinoxide anions via the ν_4 fundamental frequency at 1570 cm^{-1} (IR-on). Both images share the same logarithmic intensity scale to emphasize additional features upon IR excitation, which are indicated by arrows and labels. (c) Concatenated high-resolution spectra under IR-off (black curves) and IR-on (red curves) conditions. The IR laser was fixed near the ν_4 fundamental frequency at 1570 cm^{-1}. All high-resolution pairs are scaled such that the peak intensity of the vibrational origin in the IR-off spectrum is normalized to 1, except for one scan taken with a detachment energy below the vibrational origin. In the latter case, the spectrum is scaled such that the intensity of the 13 167 cm^{-1} feature agrees with that of the scan taken at the next higher detachment energy. (d) Corresponding difference spectra for the high-resolution spectra shown in panel (c) (IR-on − IR-off) including peak labels. Assignments are shown in Table 2. (e) Harmonic Franck−Condon simulation for photodetachment from vinoxide excited via the ν_4 fundamental. Transitions originating from the vibrational ground state in the anion are not shown.

at 1570 cm^{-1}. Note that the IR-on and IR-off images, presented with a logarithmic intensity scale, are acquired simultaneously under identical experimental conditions, which allows for a direct comparison (see Section 2). Clearly, additional ring features at larger radii appear upon vibrational excitation. The corresponding transitions are more easily seen by comparing the high-resolution cryo-SEVI spectra under IR-on and IR-off conditions in Figure 3c, which are obtained from reconstruction of the corresponding velocity-map images. Five additional peaks

appear at eBE values below the vibrational origin (A1) upon vibrational excitation. In tandem, new peaks are observed above the vibrational origin, and all peaks that are present in the ground-state spectrum are depleted upon IR excitation. The integral of the vibrational origin (peak A1), for example, decreases by ∼14.5%.

Figure 3d shows the corresponding difference spectra (IR-on − IR-off) to better distinguish additional peaks arising from IR pre-excitation (positive features) and depletion of peaks in the ground-state spectrum (negative features). To first approximation, the spectrum of the vibrationally excited molecules (Figure 3d) looks similar to the ground-state spectrum (black trace in Figure 3c) but is shifted to lower eBE, where peak B1 at 13 167 cm^{-1} marks the onset of the spectrum. Because peak B1 is shifted by −1554 cm^{-1} relative to the vibrational origin, it is assigned by inspection to the 4_1^0 transition. Closer inspection of the difference spectra (Figure 3d) reveals a progression (B1, B2, B4) with a spacing of ∼500 cm^{-1}, similar to the one in the ground-state spectrum. Peaks B5 and B7 as well as peaks B6, B8, and B9 form similar progressions with roughly the same spacing. The shapes of peaks B6, B8, and B9 are asymmetric due to overlap with nearby, depleted ground-state features, which makes a precise determination of their peak frequencies difficult. The full assignment of the features in Figure 3d, shown in Table 2 and based on the FC simulation in Figure 3e, will be discussed in Section 4.2.

Table 2. Electron Binding Energies (eBEs) and Assignments for the IR-cryo-SEVI Spectrum of Vinoxide Excited along the ν_4 Vibration

peak	eBE^a (cm^{-1})	assignment	shift to 4_1^0
B1	13 167(16)	4_1^0	0
B2	13 664(12)	$4_1^0 9_0^1$	498
B3	14 121(10)	$4_1^0 8_0^1$	954
B4	14 166(11)	$4_1^0 9_0^2$	999
B5	14 562(11)	$4_1^0 5_0^1$	1395
B6	14 701(16)^b	4_1^1	1534
B7	15 055(15)	$4_1^0 5_0^1 9_0^1$	1889
B8	15 206(16)^b	$4_1^1 9_0^1$	2040
B9	15 704(24)^b	$4_1^0 5_0^1 7_0^1$	2537
		$4_1^1 9_0^2$	
B10	15 816(13)	$4_1^1 7_0^1$	2649
B11	16 202(18)	4_1^2	3035
B12	16 315(12)	$4_1^1 7_0^1 9_0^1$	3148

^{a}Electron binding energies are determined from Gaussian fits to the highest-resolution difference spectrum for that peak, and the uncertainties in parentheses are estimated as 1σ based on the widths of the Gaussian fits unless noted otherwise. ^{b}Peak overlaps with another peak that originates from the vibrational ground state. The eBE and its uncertainty are therefore estimated based on the eBE difference between the maximum of the positive feature and the minimum of the depleted feature.

4.1.3. Pre-excitation of the C−H Stretching Mode (ν_3 IR-cryo-SEVI Spectrum).

IR-cryo-SEVI spectra of vinoxide molecules excited along the C−H stretching mode (ν_3) are shown in Figure 4a (red trace) together with the simultaneously measured ground-state spectra (black trace). The corresponding difference spectrum is shown in Figure 4b. As in Figure 3, significant depletion of the ground-state features—showing an integrated depletion of ∼33.5% for the vibrational origin—is observed and indicates strong population of the excited
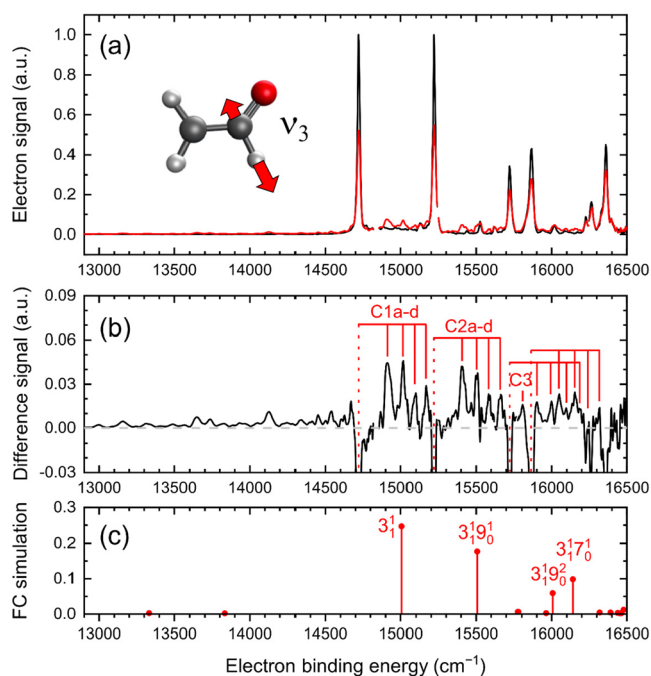
Figure 4. (a) Concatenated high-resolution spectra under IR-off (black curves) and IR-on (red curves) conditions for IR laser excitation via the ν_3 fundamental at 2546 cm^{-1}. All high-resolution pairs are scaled such that the peak intensity of the vibrational origin in the IR-off spectrum is normalized to 1. (b) Corresponding difference spectra for the high-resolution spectra shown in panel (a) (IR-on − IR-off). Combs and labels indicate groups of four peaks that are observed for each expected transition shown in panel (c). (c) Harmonic FC simulation for transitions originating from the zeroth-order ν_3 state in the anion, using deperturbed VPT2 frequencies without considering anharmonic resonances to calculate the electron binding energies.

vibrational level. In contrast to the ν_4 IR-cryo-SEVI spectrum, the ν_3 spectrum does not appear to be a shifted ground-state spectrum and is more complicated. Above the vibrational origin (A1), four intense new features on average are observed for each depleted ground-state peak, forming a quartet with a 2:2:1:1 intensity pattern. In addition, numerous low-intensity features appear at eBE values below the vibrational origin, forming a seemingly irregular spectrum.

The presence of these additional features is a consequence of strong anharmonic coupling between the ν_3 mode and several other near-resonant vibrational states in both the anion and the neutral. This is illustrated by the comparison between the difference spectrum (Figure 4b) and a FC simulation of the ν_3 zeroth-order state in the anion based on a deperturbed VPT2 calculation (Figure 4c), which does not consider anharmonic resonances. In the absence of anharmonic coupling, a single peak attributed to the 3_1^1 transition would be expected between peaks A1 and A2, owing to the slightly larger ν_3 frequency in the neutral compared to the anion. Instead, the quartet is observed. It is therefore reasonable to assume that at least some of those four peaks originate from a splitting of the 3_1^1 transition due to strong anharmonic coupling in the neutral. In addition, the experimental features at low eBE extend to at most 2000 cm^{-1} below the vibrational origin (A1). This value is much smaller than the frequency of the ν_3 CH stretching vibration, and the simulation of the spectrum does not predict any transitions with appreciable FC activity that are shifted by the ν_3 frequency. Therefore, transitions originating from the uncoupled zeroth-

order ν_3 state in the anion alone cannot explain the observed features below the vibrational origin. Those hot band transitions must instead be related to the mixed character of the nominal ν_3 state in the anion in which other zeroth-order states, e.g., overtones or combination bands, contribute through anharmonic couplings. Transitions from these coupled zeroth-order states then result in the features below the vibrational origin (A1).

4.1.4. Infrared Action Spectra of the ν_3 and ν_4 Fundamentals. Our calculations at the B2PLYP-D3/aug-cc-pVTZ level of theory including anharmonicity find two strong IR transitions for the vinoxide anion: the C−O stretch (ν_4) at 1560 cm^{-1} and the C−H stretch (ν_3) on the carbonyl at 2512 cm^{-1}.[77] Experimentally, fundamental frequencies for exciting the ν_3 and ν_4 modes in the anion have not been previously reported, and they were determined from the IR action spectra in Figure S7, which peak near the frequencies expected from our anharmonic frequency calculations. Such action spectra can be obtained with IR-cryo-SEVI by measuring the depletion or increase of the intensity of features in the IR-on spectra relative to the intensity of the vibrational origin (A1) in the IR-off spectra as a function of IR wavelength.[23] For the ν_3 vibration (Figure S7a), the spectrum is based on depletion of the vibrational origin, and the peak center is near ~2540 cm^{-1}. For the ν_4 vibration (Figure S7b), the spectrum is based on the relative increase of peak B1, and the peak center is found at 1566 cm^{-1}. Note that we did not attempt precise determination of the vibrational band centers and instead tuned the IR laser to frequencies that gave maximum depletion or absorption to obtain optimal signal from excited anions, as indicated by the arrows in Figure S7. A qualitative discussion of the shape of the IR action spectra is presented in Section S2.

4.2. Assignment of the Cryo-SEVI and IR-cryo-SEVI Spectra. *4.2.1. Ground-State Cryo-SEVI Spectrum.* We first analyze the cryo-SEVI spectrum of ground-state vinoxide before considering the IR-cryo-SEVI spectra. Electron binding energies and assignments for the ground-state cryo-SEVI spectrum (black traces in Figure 2) are shown in Table 1. The comparison of this spectrum to the previously reported SEVI spectrum without cryogenic cooling of the anion leads to some modified assignments.

The position of the vibrational origin (A1) of 14 721(8) cm^{-1} gives a slightly refined value for the adiabatic electron affinity of 1.8252(10) eV. Comparison to the assignment by Yacovitch et al.[38] and a FC simulation shown as a red stick spectrum in Figure 2 readily gives the assignment for most of the main features in the cryo-SEVI spectrum. The ~500 cm^{-1} progression involving peaks A2, A3, and A6 clearly corresponds to a progression in the CCO bending mode (9_0^1, 9_0^2, and 9_0^3), and peak A2 gives a value of 499(8) cm^{-1} for the ν_9 fundamental frequency. Peaks A5 and A7 correspond to excitation of the C−C stretching mode (7_0^1) and the C−O stretching mode (4_0^1), with fundamental frequencies of 1143(8) and 1542(9) cm^{-1}, respectively. Peak A9 corresponds to $7_0^1 9_0^1$ excitation.

Several bands that were assigned to hot band transitions in ref 38, in which anions were not cryogenically cooled, are absent in the cryo-SEVI spectrum. For example, two previously observed transitions at 14 195 and 14 918 cm^{-1}, originating from thermal excitation of the lowest-frequency ν_9 and ν_{12} modes in the anion, are not observed in the present cryo-SEVI study. We can therefore rule out that any of the smaller features labeled by "an" are related to hot band transitions. Note that the anion ν_{12} mode

was labeled as ν_{11} in ref 38, as its normal mode motion is similar to that of the neutral ν_{11} mode.

In addition, we can assign the lower-intensity features labeled by "an", which in ref 38 were either obscured by hot band transitions, incorrectly assigned as hot bands, or not identified as peaks. The $\sim$400 cm^{-1} progression in features a1, a3, and a5 matches well with the calculated frequency of the CH$_2$ twisting mode (ν_{12}). While the 12_0^2 feature (a3) is predicted by the FC simulation, 12_0^1 and 12_0^3 (a1 and a5) are odd-quanta transitions in a mode of A'' symmetry and thus symmetry-forbidden. We attribute those odd-quanta transitions to Herzberg−Teller coupling[78] between the $\tilde{X}\,^2A''$ ground state and the $\tilde{A}\,^2A'$ excited state that lies only $\sim$1 eV higher in energy. The anisotropy parameters β for the 12_0^1 transition are indeed systematically more positive than those from the FC-allowed peaks (see Figure S6), consistent with the more positive values of β observed in previous VMI photodetachment studies for the $\tilde{A}$ state vs the $\tilde{X}$ state.[37,38] For the other low-intensity peaks, the β-parameter curves are too noisy for a similar comparison. The position of peak a1 yields 408(10) cm^{-1} for the ν_{12} frequency, consistent with the experimental values of refs 48 and 53. Following a similar argument, we assign peak a2, which is shifted by 717 cm^{-1} relative to A1, to the symmetry-forbidden 11_0^1 transition, in good agreement with the anharmonic ν_{11} frequency of 728 cm^{-1} calculated in the present work. This value is also in excellent agreement with the ν_{11} hot band transition observed by Thomas et al.[48] and confirms their critical reanalysis of the ν_{11} frequency extracted from previous LIF and SEVI data. Peak a7, which shows a shift of 1373 cm^{-1} and also appears with low intensity in the FC simulation, is assigned to the 6_0^1 transition.

With the known frequency of the ν_{12} mode, we assign features a4 and a6 to the $9_0^1 12_0^1$ and $9_0^1 12_0^2$ combination bands, which are shifted from a1 and a3 by $\sim$500 cm^{-1}, respectively. The presence of Herzberg−Teller coupling for both the ν_{11} and ν_{12} modes might also explain the shoulders A4 and A8, which fit well to the expected frequencies of the $11_0^1 12_0^1$ and $9_0^1 11_0^1 12_0^1$ transitions, respectively. The $11_0^1 12_0^1$ shift further aligns well with the 1113 cm^{-1} feature in the LIF spectra of ref 53 that was reassigned to the $\nu_{11} + \nu_{12}$ combination band by Thomas et al.[48]

4.2.2. ν_4 IR-cryo-SEVI Spectrum. Because of the excellent agreement between the experimental difference spectrum (Figure 3d) and the FC simulation (Figure 3e), including only transitions that originate from the ν_4 zeroth-order state, all labeled features can be unambiguously identified. The assignment is shown in Table 2. Overall, the ν_4 IR-cryo-SEVI spectrum provides a simple case in which the initially prepared state is well-characterized by excitation of this vibration with negligible anharmonic coupling to other vibrational levels. This observation is consistent with the VPT2 calculations, which do not identify any strong resonance interactions.

As mentioned in Section 4.1, peak B1 at 13 167 cm^{-1} marks the onset of the ν_4 spectrum and is assigned to the 4_1^0 transition. The shift of the 4_1^0 transition with respect to the vibrational origin of −1554(16) cm^{-1}, reflecting the vibrational energy of the anion after IR pre-excitation, gives another measurement of the ν_4 frequency in the anion that is consistent with the band center estimated from the corresponding IR action spectrum at 1566 cm^{-1} (see Figure S7b). The spacing between peaks B1, B2, and B4 is consistent with a progression in the ν_9 mode (4_1^0, $4_1^0 9_0^1$, and $4_1^0 9_0^2$) that is also clearly seen in the FC simulation. B6, which lies close to the vibrational origin but is still partially resolved, is assigned to the 4_1^1 sequence band. Overall, these transitions

terminate in neutral levels that are also observed in the ground-state spectrum but are now shifted to lower eBE due to initial excitation of the ν_4 mode in the anion.

The above-mentioned peaks, as well as peaks B8−B12, mainly show activity in the neutral ν_4, ν_7, and ν_9 vibrations, which are already FC-active starting from the vibrational ground state. The remaining peaks (B3, B5, and B7) show FC activity in the ν_5 and ν_8 modes, which are not accessible from the vibrational ground state and become active following ν_4 excitation through Duschinsky rotation. This effect results from the differences between the normal coordinates that describe the ν_4 mode in the anion and the neutral.[74] More specifically, when the normal coordinate that describes the ν_4 mode of the anion is projected onto the normal modes of the neutral, it not only contains contributions from the neutral ν_4 mode but also the neutral ν_5 and ν_8 modes. On the basis of the FC simulation, peak B3 is assigned to the $4_0^0 8_0^1$ transition and leads to an estimate of 954(10) cm^{-1} for the ν_8 fundamental. Peaks B5 and B7 are assigned to $4_1^0 5_0^1$ and $4_1^0 5_0^1 9_0^1$, which yields a ν_5 fundamental frequency of 1395(11) cm^{-1}, in close agreement with the calculated anharmonic VPT2 frequency of 1409 cm^{-1}. However, this value differs from the ν_5 frequency reported in ref 53 (1486 cm^{-1}); this discrepancy will be discussed in Section 5.

4.2.3. ν_3 IR-cryo-SEVI Spectrum. As mentioned earlier, the harmonic FC spectrum of the zeroth-order ν_3 state (Figure 4c) is not sufficient to explain the large number of observed transitions in Figure 4b. First, we will address the transitions below the vibrational origin, which are caused by anharmonic coupling of the ν_3 fundamental in the anion. We then discuss the origin of the quartet features above the vibrational origin that are mainly caused by anharmonic coupling of ν_3 within the neutral.

The features below the vibrational origin appear in a region where hot band transitions that involve lower-frequency vibrations would normally be expected. However, the hot bands seen in the IR-cryo-SEVI spectrum cannot originate from thermally populated vibrational states as the molecules are selectively excited with a narrow $\sim$3 cm^{-1} bandwidth and no hot bands are observed in the ground-state cryo-SEVI spectrum. At the same time, the laser bandwidth is sufficiently narrow to only excite a single vibrational level instead of multiple eigenstates within the 3_1 resonant space of the anion. We thus interpret the additional transitions below the vibrational origin as contributions of various zeroth-order states that are mixed into the wave function of the nominal ν_3 eigenstate in the anion through anharmonic coupling. Inspection of the squared mixing coefficients, $|c_j''|^2$, obtained from diagonalization of the anion coupling matrix (Tables S3 and S4), indeed shows a significant contribution of the $\nu_4 + \nu_8$ zeroth-order state (28%) along with that of the ν_3 zeroth-order state (69%). Another small contribution comes from the $2\nu_6$ overtone (2%). Figure 5 illustrates how contributions from such zeroth-order dark states can enable transitions that would not be FC-allowed from the ν_3 zeroth-order bright state.

Figure 6a shows the anharmonic FC spectrum evaluated using eq 6, in which anharmonic coupling in the anion is considered while assuming that no neutral anharmonic coupling is present within the plotted region below the vibrational origin. Overall, the simulated intensities and frequencies of FC-allowed transitions (dotted line in Figure 6a) are in good agreement with the experimentally observed transitions below the vibrational origin (Figure 6b). See Section S1.2 and Table S5 for details on how the eBE values were calculated. The stick spectrum in Figure 6a thus allows us to confidently assign many
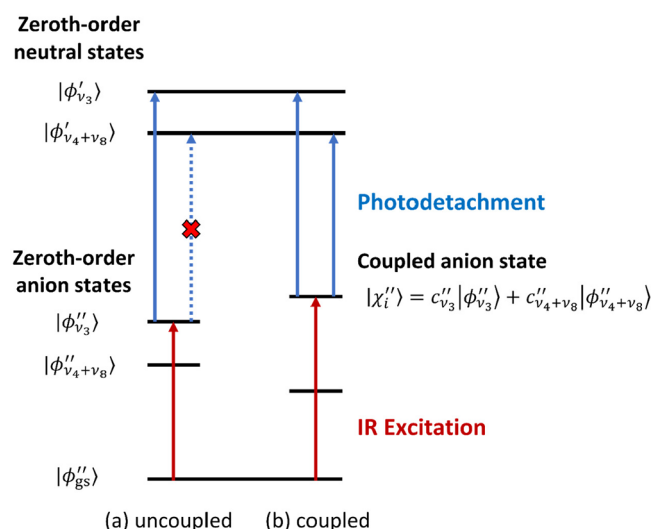
Figure 5. Schematic energy level diagram showing how additional photodetachment transitions arise due to anharmonic coupling of the ν_3 mode with other vibrational levels. Anion and neutral zeroth-order states for the uncoupled case are shown on the left (a), and the excited anharmonically coupled eigenstate in the anion is shown on the right (b). IR excitation is shown by red arrows, and detachment transitions are shown by blue arrows. The dashed arrow indicates a non-FC allowed transition. Note that only two zeroth-order states (ν_3 and $\nu_4 + \nu_8$) with the largest contributions to the coupled anion state are shown for clarity. Anharmonic coupling within the neutral is also neglected in this scheme, and neutral zeroth-order states are shown instead for both cases.

Figure 6. (a) The black stick spectrum shows the anharmonic Franck–Condon simulation for vinoxide excited via the ν_3 fundamental below the vibrational origin. Anharmonic FC factors are calculated according to eq 6, including all anion zeroth-order states, but assuming no anharmonic coupling between neutral states. The dotted line shows a convolution of the stick spectrum, offset and scaled by an arbitrary scaling factor, using an eKE-dependent linewidth as described in Section S1.3. Colored combs indicate transitions that can nominally be assigned to the $\nu_4 + \nu_8$ (blue) and ν_3 (red) anion zeroth-order states. Note that the transitions explaining peaks c3 and c8 show contributions from both the $\nu_4 + \nu_8$ and ν_3 zeroth-order states. (b) Experimental low eBE region of the ν_3 IR-cryo-SEVI difference spectrum below the vibrational origin based on the corresponding high-resolution scan from Figure 4b, which was measured at a photon energy of 14 848 cm^{-1}. Observed peaks are indicated by the combs and labels. Corresponding peak assignment can be found in Table 3.

of the experimentally observed peaks (c1–c19 in Figure 6b) to transitions from the nominal 3_1 level in the anion into different neutral states, as shown in Table 3. These neutral states all have low vibrational energy and thus are expected to exhibit negligible anharmonic coupling, justifying the use of eq 6.

Although the calculated anharmonic FC factors are extremely sensitive to the exact contributions of different anion zeroth-order states, most transitions can still be assigned to a nominal anion zeroth-order state by inspection of the FC spectra obtained for the individual anion zeroth-order states that contribute to the nominal ν_3 eigenstate, weighted by the square of the corresponding expansion coefficients. These spectra will be referred to as "weighted FC spectra". This approach corresponds to neglecting the cross-terms between different anion zeroth-order states in eq 6 when evaluating the FC spectrum and is described in Section S3. When one of the contributions to the weighted FC spectrum, shown in Figure S8, anticipates a peak in the spectrum, the nominal anion zeroth-order state is also indicated in Table 3 and above the anharmonic FC simulation in Figure 6a by colored combs. In particular, coupling to the $\nu_4 + \nu_8$ zeroth-order state explains most of the spectrum below the vibrational origin. However, some observed peaks, such as c1, c4, and c9, are not reproduced by the FC simulation and are likely attributed to an additional anharmonic resonance that is not captured by the present model. Discrepancies between the experimental and simulated spectra may further arise from the fact that harmonic zeroth-order states are used to approximate the deperturbed basis states in eq 6.

Figure 7b shows the experimentally observed structure in the vicinity of the expected 3_1^1 transition. Here, the intense quartet cannot be explained by the FC spectra based only on coupling among the anion zeroth-order states. We therefore argue that at
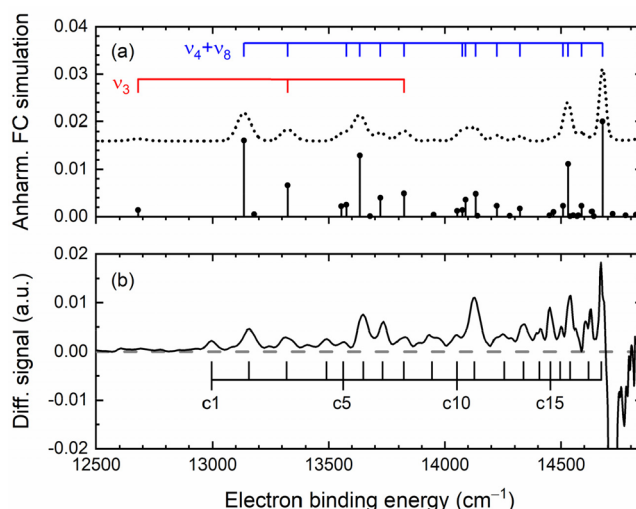
least some of the features C1a–d are caused by strong anharmonic splitting of the neutral 3^1 level. The resonant coupling space of the neutral ν_3 mode thus needs to be explicitly considered in the anharmonic FC simulations. This will be discussed in detail for the splitting of the 3_1^1 transition, but the same explanation should also hold for the splitting of the $3_1^1 9_0^1$, $3_1^1 9_0^2$, and $3_1^1 7_0^1$ transitions if we assume that the ν_7 and ν_9 modes merely act as spectator modes.

The FC simulation in Figure 7a, which includes anharmonic coupling within both the anion and the neutral according to eq 5, is in good agreement with the experimental spectrum in Figure 7b. The convolution of the simulated spectrum (dotted line in Figure 7a) shows five peaks, four of which have similar positions and relative intensities as the experiment (Figure 7b). It should again be noted that the exact values of the anharmonic FC factors are very sensitive to the anion zeroth-order state contributions. Also here, weighted FC spectra (Section S3 and Figure S9) allow us to nominally assign peaks C1a–d to different anion zeroth-order states, as indicated by the colored combs above the anharmonic FC simulation (stick spectrum in Figure 7a). Almost all transitions that contribute to peaks C1a–c can be nominally assigned to the ν_3 zeroth-order anion state (red), whereas only a small contribution to peak C1c comes from the $\nu_4 + \nu_8$ zeroth-order state (blue). Those peaks are thus mainly caused by anharmonic splitting of the neutral 3^1 level. However, peak C1d is caused by transitions that originate from the $\nu_4 + \nu_8$ zeroth-order state.

Unfortunately, the vibrational states in the 3^1 resonant space are so strongly mixed that it is difficult to make nominal state

Table 3. Electron Binding Energies (eBEs) and Assignments for the IR-cryo-SEVI Spectrum of Vinoxide Excited Along the ν_3 Vibration[a]

peak	eBE[b] (cm^{-1})	assignment (initial zeroth-order state)	assignment (final eigenstate)	shift to 3^0_1[c]
c1	12 996(19)	unassigned		815
c2	13 157(28)	$\nu_4 + \nu_8$	8^1	976
c3	13 320(30)	$\nu_4 + \nu_8/\nu_3$	7^1	1139
c4	13 490(22)	unassigned		1309
c5	13 562(20)	$2\nu_6$	6^1	1381
		$\nu_4 + \nu_8$	5^1	
c6	13 649(24)	$\nu_4 + \nu_8$	$8^1 9^1$	1468
c7	13 733(21)	$\nu_4 + \nu_8$	4^1	1552
c8	13 822(28)	$\nu_4 + \nu_8/\nu_3$	$7^1 9^1$	1641
c9	13 944(35)	unassigned		1763
c10	14 052(23)	$2\nu_6$	$6^1 9^1$	1871
		$\nu_4 + \nu_8$	$5^1 9^1$	
c11	14 127(22)	$\nu_4 + \nu_8$	8^2	1946
		$\nu_4 + \nu_8$	$8^1 9^2$	
c12	14 254(39)	$\nu_4 + \nu_8$	$4^1 9^1$	2073
c13	14 338(25)	unassigned		2157
c14	14 406(16)	unassigned		2225
c15	14 454(13)	unassigned		2273
c16	14 496(9)	$\nu_4 + \nu_8$	$6^1 8^1$	2315
c17	14 539(17)	$\nu_4 + \nu_8$	$5^1 8^1$	2358
c18	14 619(18)	unassigned		2438
c19	14 672(9)	$\nu_4 + \nu_8$	$4^1 8^1$	2491
C1a	14 918(22)	ν_3	3^1 polyad[d]	2737
C1b	15 016(18)	ν_3	3^1 polyad[d]	2835
C1c	15 091(12)	ν_3	3^1 polyad[d]	2910
C1d	15 169(14)	$\nu_4 + \nu_8$	$4^1 8^1 9^1$	2988
C2a	15 410(16)	ν_3	$3^1 9^1$ polyad[d]	3229
C2b	15 503(9)	ν_3	$3^1 9^1$ polyad[d]	3322
C2c	15 585(10)	ν_3	$3^1 9^1$ polyad[d]	3404
C2d	15 663(15)	$\nu_4 + \nu_8$	$4^1 8^1 9^2$	3482
		$\nu_4 + \nu_8$	$5^1 7^1 8^1$	
C3	15 804(11)	$\nu_4 + \nu_8$	$4^1 8^1 7^1$	3623

[a]Assignments are given for the nominal neutral vibrational eigenstates (final) and the zeroth-order anion states (initial) that contribute intensity to transitions into those final states. Initial states separated by a slash indicate that multiple anion zeroth-order states contribute intensity to a transition into the same final state. If multiple transitions into different final states contribute to an observed peak, those are written in different rows. [b]Electron binding energies are determined from Gaussian fits to the highest-resolution difference spectrum for that peak, and the uncertainties in parentheses are estimated as 1σ based on the widths of the Gaussian fits. [c]The 3^0_1 transition frequency is estimated as $EA - \nu_{3,anion} = 12\,181$ cm^{-1}, where the electron affinity is $EA = 14\,721$ cm^{-1} and the anion frequency is estimated as $\nu_{3,anion} = 2540$ cm^{-1}. [d]See main text for more details on the states involved in the 3^1 polyad.

assignments. Only the intense peak at 2723 cm^{-1} in Figure 7a, which contributes to C1a, has clearly dominant $2\nu_6$ character. The other states that contribute to peaks C1a−C1c mostly show contributions from several resonant neutral states that can be found in the coefficient matrix in the Supporting Information. As no definite assignments to nominal states can be given, we will collectively refer to peaks C1a−C1c as a 3^1 polyad in Table 3.[79,80] The same splitting due to the polyad structure is also expected for the other transitions, $3^1_1 9^1_0$, $3^1_1 9^2_0$, and $3^1_1 7^1_0$. The corresponding peaks will therefore be assigned to $3^1 9^1$, $3^1 9^2$, and $3^1 7^1$ polyads.
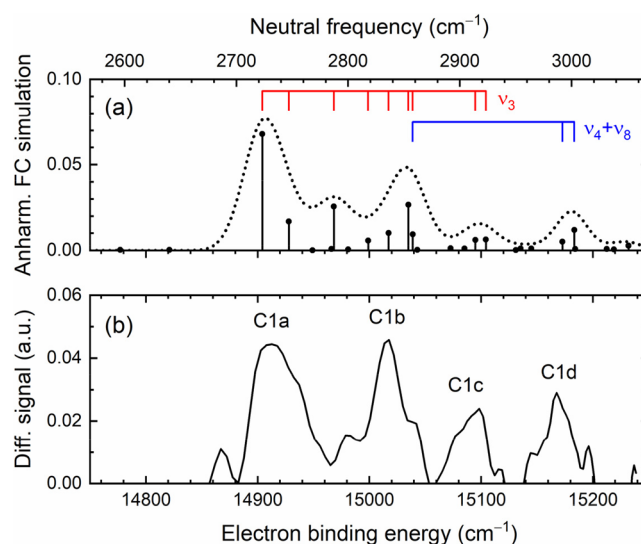

Figure 7. (a) The black stick spectrum shows the anharmonic Franck−Condon simulation for vinoxide excited via the ν_3 fundamental in the eBE region near the expected 3^1_1 transition, calculated according to eq 5 in which anharmonic coupling for both the anion and neutral ν_3 modes is included. The dotted line shows a convolution of the stick spectrum, scaled by an arbitrary scaling factor and using an eKE-dependent linewidth as described in Section S1.3. Colored combs indicate transitions that can nominally be assigned to the ν_3 (red) and $\nu_4 + \nu_8$ (blue) anion zeroth-order states. Neutral frequencies shown at the top are related to the eBE by a shift of $-EA + \nu_{3,anion} = -12\,181$ cm^{-1}, where the electron affinity is $EA = 14\,721$ cm^{-1} and the anion frequency is estimated as $\nu_{3,anion} = 2540$ cm^{-1}. (b) Experimental difference spectrum near the expected 3^1_1 transition based on the corresponding high-resolution scan from Figure 4b, which was measured at a photon energy of 15 290 cm^{-1}.

5. DISCUSSION

The fundamental frequencies of the vinoxy radical extracted from the cryo-SEVI and IR-cryo-SEVI spectra are summarized in Table 4, together with the calculated VPT2 frequencies and other experimental values from the literature. For most frequencies, the agreement with the most recent experimental data is within our estimated error limits. The ν_5 frequency of 1395(11) cm^{-1} determined in this work, on the other hand, clearly deviates from the best estimate of 1486 cm^{-1} obtained through LIF spectroscopy.[51,53] Also the splitting of the 3^1_1 peak into three features has not been previously observed. However, the frequency of 2835(18) cm^{-1}, extracted from the central peak C1b, is consistent with the band center determined in ref 55, the only other report of the ν_3 frequency.

The comparison between the ν_4 IR-cryo-SEVI spectrum and the FC simulation in Figure 3 allows us to unambiguously determine the ν_5 frequency from peaks B5 and B7. In addition, our VPT2 frequency calculations including anharmonic resonances predict a value of 1409 cm^{-1}, which lies almost within the error of our experimental value. This calculated value is also in line with the more recent MRCISD calculation by Yamaguchi et al.,[54] who reported a scaled harmonic frequency of 1441 cm^{-1}, and anharmonic VPT2 calculations by Thomas et al.[48] at the B3LYP/aug-cc-pVTZ level of theory, providing a value of 1392 cm^{-1}. The discrepancy between our value of 1395(11) cm^{-1} for the ν_5 fundamental frequency and other measurements therefore most likely results from previous assignments being based on harmonic frequency values.

Table 4. Fundamental Frequencies of the Vinoxy Radical Determined in this Work, Calculated VPT2 Frequencies at the B2PLYP-D3/aug-cc-pVTZ Level of Theory, and Most Recent Experimentally Determined Literature Values

mode	this work	source[a]	VPT2	ref 48	ref 55	ref 53	ref 38	ref 51[h]
ν_1			3147					
ν_2			3057					
	2737(22)							
ν_3	2835(18)	ν_3	2806[b]		2827.91259(3)			
	2910(12)							
ν_4	1542(9)	SEVI	1545[c]			1543	1528	1540
ν_5	1395(11)	ν_4	1409			1486[e]		1454
ν_6	1373(15)	SEVI	1374			1366		1361
ν_7	1143(8)	SEVI	1132			1143	1137	1141
ν_8	954(10)	ν_4	955			957		949
ν_9	499(8)	SEVI	501			500	498	498
ν_{10}			971			703[f,g]		
ν_{11}	717(6)	SEVI	728	717[d]		557[f,g]		
ν_{12}	408(10)	SEVI	399	402		404[g]		

[a]Indicates whether the frequency in the present work is extracted from the ground-state cryo-SEVI spectrum (SEVI) or the IR-cryo-SEVI spectra (ν_3 or ν_4). [b]There is no nominal ν_3 frequency due to the strong anharmonic coupling involving this mode (see main text). Instead, the deperturbed VPT2 value is reported. [c]The harmonic frequency of the ν_4 mode has been shifted by -50 cm^{-1} to achieve this result for the fundamental frequency. Without this shift in the harmonic frequency, the calculated anharmonic fundamental frequency is 1591 cm^{-1}. [d]On the basis of the ν_{11} hotband observed in ref 48, not the estimate from ref 48 based on the data from ref 38. [e]Potentially the upper level of the $\nu_5/2\nu_{11}$ Fermi pair (see main text). [f]These transitions were likely misassigned based on the more recent experiments and calculations. [g]Estimated as half of the overtone frequency in ref 53. [h]Reanalysis of the LIF data collected before 1990.

Considering how well our calculated VPT2 frequencies agree with all of the other fundamental frequencies, it is likely that the ν_5 fundamental frequency and its resonances with nearby vibrational states are also described correctly. This allows us to identify the origin of its anharmonic shift. The resonant space of the ν_5 mode in the neutral shows a strong Fermi resonance between the ν_5 fundamental and the $2\nu_{11}$ overtone, with a coupling matrix element of 38.3 cm^{-1}, along with other weaker resonances (see Table S6). This Fermi resonance results in two calculated levels at 1409 and 1494 cm^{-1} with dominant ν_5 and $2\nu_{11}$ character, respectively (Table S7). The photodetachment transition into the upper level, expected at an eBE of 14 662 cm^{-1}, cannot be clearly identified in the IR-cryo-SEVI spectrum because it would partially overlap with the 4_1^1 feature and the depleted vibrational origin. We speculate that the 1486 cm^{-1} level, which was assigned to the ν_5 fundamental by Brock and Rohlfing,[53] belongs to the upper level of the Fermi resonance pair. On the other hand, no transition for the lower level with comparable intensity is reported at a shift of ~1395 cm^{-1} in ref 53.

We now discuss the strong anharmonic splitting within the 3^1 polyad of the vinoxy radical, with peaks at 2737(22), 2835(18), and 2910(12) cm^{-1} (C1a–C1c). The ν_3 mode shows a comparatively isolated vibration, mainly involving motion of the C–H bond, while structural changes during photodetachment from the vibrational ground state primarily occur within the C–C–O backbone (see Table S1). The same is true for $\tilde{B}^2A'' \rightarrow \tilde{X}^2A''$ fluorescence experiments where the C–H bond distances remain almost unchanged in the $\tilde{B}$ state.[36,38,40,54] The ν_3 mode as well as the other two C–H stretching vibrations are therefore not FC-active in any of those experiments, and it should generally be easier to observe them with IR spectroscopy. There, a comparable redistribution of the ν_3 oscillator strength across different neutral vibrations as in the red stick spectrum in Figure S9b would be expected due to anharmonic coupling. However, only two such IR absorption studies exist to the best of our knowledge. In an argon matrix isolation study, a germanium

filter with a cutoff of ~2000 cm^{-1} was used to avoid changes within the sample while exposing it to the IR radiation, which prevented measurements of the C–H stretching vibrations.[44] In the second experiment by Utkin et al.,[55] a high-resolution gas-phase study, the observation of transitions at 2737(22) and 2910(12) cm^{-1} (C1a and C1c, respectively) should have been possible in principle, but the authors only reported the center peak at 2827.91259(3) cm^{-1} (C1b). Their data for jet-cooled vinoxy has only been collected in the 2809–2860 cm^{-1} range, where rovibrational transitions from the two coupled vibrations would likely not be observed. Their room-temperature spectrum was measured over a larger range of 2754–2894 cm^{-1} but is also more congested, which might explain why the anharmonic resonances could not be identified. On the other hand, Utkin et al. did note that perturbations with nearby vibrational levels exist and that many transitions originating from about half of the observed K'_a levels seem to be systematically perturbed, which might be a result of the strong anharmonic coupling reported in the present work.

The high frequency of the excited ν_3 mode in the anion and neutral, associated with a higher vibrational state density,[81] facilitates anharmonic coupling, in notable contrast to excitation of the lower-frequency ν_4 mode. Despite the strong coupling present in the ν_3 IR-cryo-SEVI spectra, anharmonic FC simulations enable us to identify specific zeroth-order dark state contributions to the nominal ν_3 mode in the anion (Figure 6) as well as vibrational eigenstates with ν_3 character in the neutral (Figure 7). Therefore, IR-cryo-SEVI has features in common with other spectrally resolved techniques that are used to probe anharmonic coupling in electronic ground states.[24−26] It is worth noting that in IR-cryo-SEVI the information on coupling within the anion and neutral ground states is spectrally separated into two eBE regions. Further note that we based our current analysis solely on vibrational coupling and did not consider the effect of the rovibrational structure, which can potentially alter the relative intensities of contributions from the ν_3 zeroth-order bright state and other zeroth-order dark states. A

similar, temperature-dependent effect is, for example, seen in IR fluorescence experiments that probe anharmonic coupling of other C−H stretching vibrations.[82,83]

The observation of the ν_3, ν_5, and ν_8 modes in the neutral, which are not accessible from the anion ground state, highlights another benefit of the IR-cryo-SEVI technique. As explained earlier, excitation of the ν_4 mode, which shares the same symmetry as the vibrational ground state, gives rise to distinctive FC activity in the ν_5 and ν_8 modes due to Duschinsky mixing,[74] in addition to activity in the ν_4, ν_7, and ν_9 modes seen in the IR-off spectrum. Besides this approach of accessing otherwise inactive neutral vibrations through the Duschinsky effect, the excitation of modes of different symmetry to access non-totally symmetric modes in the neutral will be another promising direction for future experiments. Such experiments could, for example, include the isomerization dynamics of vinylidene to acetylene, which mainly involves the ν_5 and ν_6 modes of neutral vinylidene, where both modes are of b_2 symmetry and could only be observed as weak transitions due to Herzberg−Teller coupling in previous cryo-SEVI studies.[84]

Finally, it is worth noting that the approach taken here to simulate the IR-cryo-SEVI spectrum is straightforward, general, and computationally efficient. It is built off of the harmonic FC treatment that is typically used to analyze spectra with transitions originating from the vibrational ground state of the anion. In this approach, vibrational perturbation theory is used to develop a basis of states that are nearly degenerate with the state of interest along with their deperturbed energies. One can then analyze the spectrum in terms of this limited vibrational basis, where the associated vibrational wave functions are treated within the harmonic approximation. With this in place, the IR-cryo-SEVI spectrum may be modeled using the FC factors evaluated based on the harmonic zeroth-order states. While similar approaches to the evaluation of anharmonic FC factors have been previously used based on anharmonic wave functions obtained from variational calculations,[75,76] those methods are computationally expensive for large molecules. For covalently bound systems like vinoxide or vinoxy where vibrational perturbation theory is generally effective, our method provides a simple approach for disentangling the complicated spectral effects of anharmonic coupling in both the anionic and neutral species.

6. CONCLUSION

The presented high-resolution photoelectron spectra of vibrationally excited vinoxide anions show the first application of IR-cryo-SEVI to a polyatomic molecule. The IR-cryo-SEVI spectrum of vinoxide excited along the C−O stretching mode (ν_4) is well-described within the harmonic approximation, indicating that anharmonic coupling in the anion is negligible for that mode. Furthermore, transitions into the ν_5 and ν_8 modes in the neutral, which are not accessible from the vibrational ground state, are observed after ν_4 excitation, allowing us to extract their fundamental frequencies. For the ν_5 mode, existing literature values differ from our measurement at 1395(11) cm^{-1}. This discrepancy is explained by a strong Fermi resonance between the ν_5 fundamental and the $2\nu_{11}$ overtone, resulting in a lower level at 1395 cm^{-1} and an upper level expected near 1490 cm^{-1}. The latter feature is not explicitly observed in our experiment but lies close to the value reported in previous work.

The IR-cryo-SEVI spectrum of vinoxide excited along the isolated C−H stretching mode (ν_3) is more complex and is explained by anharmonic coupling of the ν_3 fundamental with other nearly degenerate vibrations in the anion and the neutral. The measured ν_3 IR-cryo-SEVI spectra are qualitatively reproduced by anharmonic Franck−Condon simulations. The effects of anharmonicity are included through nearly degenerate vibrational perturbation theory, and the resultant nearly degenerate states serve as a basis within the context of anharmonic Franck−Condon simulations. The analysis shows that many observed hot band transitions can be explained by anharmonic coupling within the anion electronic ground state. Furthermore, a polyad comprising three distinct features at 2737(22), 2835(18), and 2910(12) cm^{-1} instead of a single feature is reported for the ν_3 fundamental in the neutral, indicating strong anharmonic resonances that are also reproduced by the Franck−Condon simulations.

Overall, the reported IR-cryo-SEVI and ground-state cryo-SEVI measurements presented here allow us to measure 9 of the 12 fundamental frequencies of the vinoxy radical (except for ν_1, ν_2, and ν_{10}) with a single experimental setup. In addition, the vibrational frequencies of the ν_4 and ν_3 fundamentals in the anion are found near 1566 and 2540 cm^{-1} using IR-cryo-SEVI as an action spectroscopy technique. The well-resolved IR-cryo-SEVI spectra—especially considering the strong coupling within the ν_3 mode—suggest that many more applications to other polyatomic systems are now possible.

■ ASSOCIATED CONTENT

ⓢ Supporting Information

The Supporting Information is available free of charge at https://pubs.acs.org/doi/10.1021/acs.jpca.3c00484.

> Additional experimental and theoretical details, details of the anharmonic Franck−Condon simulations, discussion of the IR action spectra, a description of the weighted FC spectra method, experimental setup, normal modes, FC simulations for different frequency shifts, anisotropy parameters, infrared action spectra, weighted FC spectra, optimized geometries in valence and Cartesian coordinates, anion ν_3 coupling and coefficient matrices, fundamental frequencies used in eBE calculations for the ν_3 simulations, and neutral ν_5 coupling and coefficient matrices (PDF)

> Coupling and coefficient matrices for the ν_3 fundamental in the anion and neutral as well as the neutral ν_5 fundamental (XLSX)

■ AUTHOR INFORMATION

Corresponding Author

Daniel M. Neumark − *Department of Chemistry, University of California, Berkeley, California 94720, United States; Chemical Sciences Division, Lawrence Berkeley National Laboratory, Berkeley, California 94720, United States;* ⓞ orcid.org/0000-0002-3762-9473; Email: dneumark@berkeley.edu

Authors

Jascha A. Lau − *Department of Chemistry, University of California, Berkeley, California 94720, United States;* ⓞ orcid.org/0000-0003-0068-373X

Martin DeWitt − *Department of Chemistry, University of California, Berkeley, California 94720, United States;* ⓞ orcid.org/0000-0002-1559-2112

Mark A. Boyer − *Department of Chemistry, University of Washington, Seattle, Washington 98195, United States;*

Present Address: Department of Chemistry, University of Wisconsin—Madison, Madison, Wisconsin 53706, United States

Mark C. Babin − *Department of Chemistry, University of California, Berkeley, California 94720, United States;* Present Address: Department of Chemistry and Chemical Biology, Harvard University, Cambridge, Massachusetts 02138, United States; ◉ orcid.org/0000-0001-7440-8058

Tonia Solomis − *Department of Chemistry, University of California, Berkeley, California 94720, United States;* ◉ orcid.org/0000-0002-4857-3495

Max Grellmann − *Wilhelm-Ostwald-Institut für Physikalische und Theoretische Chemie, Universität Leipzig, 04103 Leipzig, Germany*

Knut R. Asmis − *Wilhelm-Ostwald-Institut für Physikalische und Theoretische Chemie, Universität Leipzig, 04103 Leipzig, Germany;* ◉ orcid.org/0000-0001-6297-5856

Anne B. McCoy − *Department of Chemistry, University of Washington, Seattle, Washington 98195, United States;* ◉ orcid.org/0000-0001-6851-6634

Complete contact information is available at:
https://pubs.acs.org/10.1021/acs.jpca.3c00484

Author Contributions

[⊥] J.A.L. and M.D. contributed equally to this work.

Notes

The authors declare no competing financial interest.

■ REFERENCES

(1) Ellison, G. B.; Engelking, P. C.; Lineberger, W. C. An Experimental Determination of the Geometry and Electron Affinity of CH₃. *J. Am. Chem. Soc.* **1978**, *100*, 2556−2558.

(2) Ichino, T.; Wren, S. W.; Vogelhuber, K. M.; Gianola, A. J.; Lineberger, W. C.; Stanton, J. F. The Vibronic Level Structure of the Cyclopentadienyl Radical. *J. Chem. Phys.* **2008**, *129*, 084310.

(3) Posey, L. A.; Deluca, M. J.; Johnson, M. A. Demonstration of a pulsed photoelectron spectrometer on mass-selected negative ions: O⁻, O₂⁻, and O₄⁻. *Chem. Phys. Lett.* **1986**, *131*, 170−174.

(4) Cheshnovsky, O.; Taylor, K. J.; Conceicao, J.; Smalley, R. E. Ultraviolet Photoelectron Spectra of Mass-Selected Copper Clusters: Evolution of the 3d Band. *Phys. Rev. Lett.* **1990**, *64*, 1785−1788.

(5) Castleman, A. W.; Bowen, K. H. Clusters: Structure, Energetics, and Dynamics of Intermediate States of Matter. *J. Phys. Chem.* **1996**, *100*, 12911−12944.

(6) Wu, H. B.; Desai, S. R.; Wang, L. S. Evolution of the Electronic Structure of Small Vanadium Clusters from Molecular to Bulklike. *Phys. Rev. Lett.* **1996**, *77*, 2436−2439.

(7) Lineberger, W. C. Once Upon Anion: A Tale of Photodetachment. *Annu. Rev. Phys. Chem.* **2013**, *64*, 21−36.

(8) Continetti, R. E.; Guo, H. Dynamics of Transient Species Via Anion Photodetachment. *Chem. Soc. Rev.* **2017**, *46*, 7650−7667.

(9) Weichman, M. L.; Neumark, D. M. Slow Photoelectron Velocity-Map Imaging of Cryogenically Cooled Anions. *Annu. Rev. Phys. Chem.* **2018**, *69*, 101−124.

(10) Rienstra-Kiracofe, J. C.; Tschumper, G. S.; Schaefer, H. F.; Nandi, S.; Ellison, G. B. Atomic and Molecular Electron Affinities: Photoelectron Experiments and Theoretical Computations. *Chem. Rev.* **2002**, *102*, 231−282.

(11) Signorell, R.; Merkt, F. General Symmetry Selection Rules for the Photoionization of Polyatomic Molecules. *Mol. Phys.* **1997**, *92*, 793−804.

(12) Mabbs, R.; Grumbling, E. R.; Pichugin, K.; Sanov, A. Photoelectron Imaging: An Experimental Window into Electronic Structure. *Chem. Soc. Rev.* **2009**, *38*, 2169−2177.

(13) Osterwalder, A.; Nee, M. J.; Zhou, J.; Neumark, D. M. High Resolution Photodetachment Spectroscopy of Negative Ions Via Slow Photoelectron Imaging. *J. Chem. Phys.* **2004**, *121*, 6317−6322.

(14) Hock, C.; Kim, J. B.; Weichman, M. L.; Yacovitch, T. I.; Neumark, D. M. Slow Photoelectron Velocity-Map Imaging Spectroscopy of Cold Negative Ions. *J. Chem. Phys.* **2012**, *137*, 244201.

(15) Weichman, M. L.; DeVine, J. A.; Levine, D. S.; Kim, J. B.; Neumark, D. M. Isomer-Specific Vibronic Structure of the 9-, 1-, and 2-Anthracenyl Radicals Via Slow Photoelectron Velocity-Map Imaging. *Proc. Natl. Acad. Sci. U.S.A.* **2016**, *113*, 1698−1705.

(16) Kim, J. B.; Weichman, M. L.; Neumark, D. M. Structural Isomers of Ti₂O₄ and Zr₂O₄ Anions Identified by Slow Photoelectron Velocity-Map Imaging Spectroscopy. *J. Am. Chem. Soc.* **2014**, *136*, 7159−7168.

(17) Weichman, M. L.; Kim, J. B.; DeVine, J. A.; Levine, D. S.; Neumark, D. M. Vibrational and Electronic Structure of the α- and β-Naphthyl Radicals Via Slow Photoelectron Velocity-Map Imaging. *J. Am. Chem. Soc.* **2015**, *137*, 1420−1423.

(18) Wörner, H. J.; van der Veen, R.; Merkt, F. Jahn-Teller Effect in the Methane Cation: Rovibronic Structure and the Geometric Phase. *Phys. Rev. Lett.* **2006**, *97*, 173003.

(19) Xing, X.; Bahng, M.-K.; Reed, B.; Lam, C. S.; Lau, K.-C.; Ng, C. Y. Rovibrationally Selected and Resolved Pulsed Field Ionization-Photoelectron Study of Propyne: Ionization Energy and Spin-Orbit Interaction in Propyne Cation. *J. Chem. Phys.* **2008**, *128*, 094311.

(20) Kasdan, A.; Herbst, E.; Lineberger, W. C. Laser Photoelectron Spectrometry of CH⁻. *Chem. Phys. Lett.* **1975**, *31*, 78−82.

(21) Engelking, P. C.; Lineberger, W. C. Laser Photoelectron Spectrometry of NH⁻: Electron Affinity and Intercombination Energy Difference in NH. *J. Chem. Phys.* **1976**, *65*, 4323−4324.

(22) Goldfarb, F.; Drag, C.; Chaibi, W.; Kröger, S.; Blondel, C.; Delsart, C. Photodetachment Microscopy of the P, Qₜ and R Branches of the OH⁻(v = 0) to OH(v = 0) Detachment Threshold. *J. Chem. Phys.* **2005**, *122*, 014308.

(23) DeWitt, M.; Babin, M. C.; Neumark, D. M. High-Resolution Photoelectron Spectroscopy of Vibrationally Excited OH⁻. *J. Phys. Chem. A* **2021**, *125*, 7260−7265.

(24) McDonald, J. D. Creation and Disposal of Vibration Energy in Polyatomic Molecules. *Annu. Rev. Phys. Chem.* **1979**, *30*, 29−50.

(25) Lehmann, K. K.; Scoles, G.; Pate, B. H. Intramolecular Dynamics from Eigenstate-Resolved Infrared-Spectra. *Annu. Rev. Phys. Chem.* **1994**, *45*, 241−274.

(26) Nesbitt, D. J.; Field, R. W. Vibrational Energy Flow in Highly Excited Molecules: Role of Intramolecular Vibrational Redistribution. *J. Phys. Chem.* **1996**, *100*, 12735−12756.

(27) Gozem, S.; Krylov, A. I. The Ezspectra Suite: An Easy-to-Use Toolkit for Spectroscopy Modeling. *WIREs Computational Molecular Science* **2022**, *12*, e1546.

(28) Wojcik, P.; Gozem, S.; Mozhayskiy, V.; Krylov, A. I. ezFCF. http://iopenshell.usc.edu/downloads (accessed August 15, 2022).

(29) Nielsen, H. H. The Vibration-Rotation Energies of Polyatomic Molecules Part II. Accidental Degeneracies. *Phys. Rev.* **1945**, *68*, 181–191.

(30) Nielsen, H. H. The Vibration-Rotation Energies of Molecules. *Rev. Mod. Phys.* **1951**, *23*, 90–136.

(31) Franke, P. R.; Stanton, J. F.; Douberly, G. E. How to VPT2: Accurate and Intuitive Simulations of CH Stretching Infrared Spectra Using VPT2+K with Large Effective Hamiltonian Resonance Treatments. *J. Phys. Chem. A* **2021**, *125*, 1301–1324.

(32) Zimmerman, A. H.; Reed, K. J.; Brauman, J. I. Photodetachment of Electrons from Enolate Anions. Gas Phase Electron Affinities of Enolate Radicals. *J. Am. Chem. Soc.* **1977**, *99*, 7203–7209.

(33) Jackson, R. L.; Hiberty, P. C.; Brauman, J. I. Threshold Resonances in the Electron Photodetachment Spectrum of Acetaldehyde Enolate Anion. Evidence for a Low-Lying, Dipole-Supported State. *J. Chem. Phys.* **1981**, *74*, 3705–3712.

(34) Ellison, G. B.; Engelking, P. C.; Lineberger, W. C. Photoelectron Spectroscopy of Alkoxide and Enolate Negative Ions. *J. Phys. Chem.* **1982**, *86*, 4873–4878.

(35) Mead, R. D.; Lykke, K. R.; Lineberger, W. C.; Marks, J.; Brauman, J. I. Spectroscopy and Dynamics of the Dipole-Bound State of Acetaldehyde Enolate. *J. Chem. Phys.* **1984**, *81*, 4883–4892.

(36) Alconcel, L. S.; Deyerl, H.-J.; Zengin, V.; Continetti, R. E. Structure and Energetics of Vinoxide and the $X(^2A'')$ and $A(^2A')$ Vinoxy Radicals. *J. Phys. Chem. A* **1999**, *103*, 9190–9194.

(37) Bowen, M. S.; Continetti, R. E. Photodetachment Imaging Study of the Vinoxide Anion. *J. Phys. Chem. A* **2004**, *108*, 7827–7831.

(38) Yacovitch, T. I.; Garand, E.; Neumark, D. M. Slow Photoelectron Velocity-Map Imaging Spectroscopy of the Vinoxide Anion. *J. Chem. Phys.* **2009**, *130*, 244309.

(39) Cvetanovic, R. J.; Singleton, D. L. Reaction of Oxygen Atoms with Olefins. *Rev. Chem. Intermed.* **1984**, *5*, 183–226.

(40) Osborn, D. L.; Choi, H.; Mordaunt, D. H.; Bise, R. T.; Neumark, D. M.; Rohlfing, C. M. Fast Beam Photodissociation Spectroscopy and Dynamics of the Vinoxy Radical. *J. Chem. Phys.* **1997**, *106*, 3049–3066.

(41) Su, H.; Bersohn, R. Vibrational State Distribution and Relaxation of Vinoxy Radicals. *J. Chem. Phys.* **2001**, *115*, 217–224.

(42) Miller, J. L.; McCunn, L. R.; Krisch, M. J.; Butler, L. J.; Shu, J. Dissociation of the Ground State Vinoxy Radical and Its Photolytic Precursor Chloroacetaldehyde: Electronic Nonadiabaticity and the Suppression of the H+Ketene Channel. *J. Chem. Phys.* **2004**, *121*, 1830–1838.

(43) Senosiain, J. P.; Klippenstein, S. J.; Miller, J. A. Pathways and Rate Coefficients for the Decomposition of Vinoxy and Acetyl Radicals. *J. Phys. Chem. A* **2006**, *110*, 5772–5781.

(44) Jacox, M. E. The Reaction of F Atoms with Acetaldehyde and Ethylene Oxide. Vibrational Spectra of the CH_3CO and CH_2CHO Free Radicals Trapped in Solid Argon. *Chem. Phys.* **1982**, *69*, 407–422.

(45) Botschwina, P. Accurate Equilibrium Structures for Small Polyatomic Molecules, Radicals and Carbenes. *Mol. Phys.* **2005**, *103*, 1441–1460.

(46) Endo, Y.; Saito, S.; Hirota, E. The Microwave Spectrum of the Vinoxy Radical. *J. Chem. Phys.* **1985**, *83*, 2026–2034.

(47) Endo, Y.; Nakajima, M. Fourier-Transform Microwave Spectroscopy of the Vinoxy Radical, CH_2CHO. *J. Mol. Spectrosc.* **2014**, *301*, 15–19.

(48) Thomas, P. S.; Chhantyal-Pun, R.; Kline, N. D.; Miller, T. A. The $\tilde{A}$-$\tilde{X}$ Absorption of Vinoxy Radical Revisited: Normal and Herzberg–Teller Bands Observed Via Cavity Ringdown Spectroscopy. *J. Chem. Phys.* **2010**, *132*, 114302.

(49) Inoue, G.; Akimoto, H. Laser-Induced Fluorescence of the C_2H_3O Radical. *J. Chem. Phys.* **1981**, *74*, 425–433.

(50) Dimauro, L. F.; Heaven, M.; Miller, T. A. Laser-Induced Fluorescence Study of the $B\ ^2A'' \rightarrow X\ ^2A''$ Transition of the Vinoxy Radical in a Supersonic Free Jet Expansion. *J. Chem. Phys.* **1984**, *81*, 2339–2346.

(51) Yamaguchi, M.; Momose, T.; Shida, T. Vibrational Analysis and Calculation of Franck-Condon Factors for the Vinoxy Radical $X(^2A'')$ and $B(^2A'')$ States. *J. Chem. Phys.* **1990**, *93*, 4211–4222.

(52) Wan, R.; Chen, X.; Wu, F.; Weiner, B. R. Observation of New Vibronic Transitions in the $\tilde{B}\ ^2A'' - \tilde{X}\ ^2A''$ Manifold of the CH_2CHO Radical. *Chem. Phys. Lett.* **1996**, *260*, 539–544.

(53) Brock, L. R.; Rohlfing, E. A. Spectroscopic Studies of the $B\ ^2A''$-$X\ ^2A''$ System of the Jet-Cooled Vinoxy Radical. *J. Chem. Phys.* **1997**, *106*, 10048–10065.

(54) Yamaguchi, M.; Inomata, S.; Washida, N. Multireference Configuration Interaction Calculation of the $\tilde{B}^2A''-\tilde{X}^2A''$ Transition of Halogen- and Methyl-Substituted Vinoxy Radicals. *J. Phys. Chem. A* **2006**, *110*, 12419–12426.

(55) Utkin, Y. G.; Han, J. X.; Sun, F. G.; Chen, H. B.; Scott, G.; Curl, R. F. High-Resolution Jet-Cooled and Room Temperature Infrared Spectra of the ν_3 CH Stretch of Vinoxy Radical. *J. Chem. Phys.* **2003**, *118*, 10470–10476.

(56) Yacovitch, T. I.; Garand, E.; Neumark, D. M. Slow Photoelectron Velocity-Map Imaging of the I-Methylvinoxide Anion. *J. Phys. Chem. A* **2010**, *114*, 11091–11099.

(57) Yacovitch, T. I.; Kim, J. B.; Garand, E.; van der Poll, D. G.; Neumark, D. M. Slow Photoelectron Velocity-Map Imaging Spectroscopy of the N-Methylvinoxide Anion. *J. Chem. Phys.* **2011**, *134*, 134307.

(58) Even, U.; Jortner, J.; Noy, D.; Lavie, N.; Cossart-Magos, C. Cooling of Large Molecules Below 1 K and He Clusters Formation. *J. Chem. Phys.* **2000**, *112*, 8068–8071.

(59) Wiley, W. C.; McLaren, I. H. Time-of-Flight Mass Spectrometer with Improved Resolution. *Rev. Sci. Instrum.* **1955**, *26*, 1150–1157.

(60) DeWitt, M.; Babin, M. C.; Lau, J. A.; Solomis, T.; Neumark, D. M. High Resolution Photoelectron Spectroscopy of the Acetyl Anion. *J. Phys. Chem. A* **2022**, *126*, 7962–7970.

(61) Dick, B. Inverting Ion Images without Abel Inversion: Maximum Entropy Reconstruction of Velocity Maps. *Phys. Chem. Chem. Phys.* **2014**, *16*, 570–580.

(62) Blondel, C.; Chaibi, W.; Delsart, C.; Drag, C.; Goldfarb, F.; Kröger, S. The Electron Affinities of O, Si, and S Revisited with the Photodetachment Microscope. *Eur. Phys. J. D* **2005**, *33*, 335–342.

(63) Cooper, J.; Zare, R. N. Angular Distribution of Photoelectrons. *J. Chem. Phys.* **1968**, *48*, 942–943.

(64) Sanov, A. Laboratory-Frame Photoelectron Angular Distributions in Anion Photodetachment: Insight into Electronic Structure and Intermolecular Interactions. *Annu. Rev. Phys. Chem.* **2014**, *65*, 341–363.

(65) Barone, V. Anharmonic Vibrational Properties by a Fully Automated Second-Order Perturbative Approach. *J. Chem. Phys.* **2005**, *122*, 014108.

(66) Boyer, M. A.; McCoy, A. B. *PyVibPTn, a general package for vibrational perturbation theory*; Zenodo: 2021; DOI: 10.5281/zenodo.5563090 (accessed July 1, 2022).

(67) Boyer, M. A.; McCoy, A. B. A Flexible Approach to Vibrational Perturbation Theory Using Sparse Matrix Methods. *J. Chem. Phys.* **2022**, *156*, 054107.

(68) Frisch, M. J.; Trucks, G. W.; Schlegel, H. B.; Scuseria, G. E.; Robb, M. A.; Cheeseman, J. R.; Scalmani, G.; Barone, V.; Petersson, G. A.; Nakatsuji, H.; et al. *Gaussian 16, Revision C.01*; Gaussian, Inc.: Wallingford, CT, 2016.

(69) Hansen, A. S.; Bhagde, T.; Qian, Y.; Cavazos, A.; Huchmala, R. M.; Boyer, M. A.; Gavin-Hanner, C. F.; Klippenstein, S. J.; McCoy, A. B.; Lester, M. I. Infrared Spectroscopic Signature of a Hydroperoxyalkyl Radical (●QOOH). *J. Chem. Phys.* **2022**, *156*, 014301.

(70) Krasnoshchekov, S. V.; Stepanov, N. F. Polyad Quantum Numbers and Multiple Resonances in Anharmonic Vibrational Studies of Polyatomic Molecules. *J. Chem. Phys.* **2013**, *139*, 184101.

(71) Boyer, M. A.; McCoy, A. B. A Wave Function Correction-Based Approach to the Identification of Resonances for Vibrational Perturbation Theory. *J. Chem. Phys.* **2022**, *157*, 164113.

(72) Yang, Q.; Bloino, J. An Effective and Automated Processing of Resonances in Vibrational Perturbation Theory Applied to Spectroscopy. *J. Phys. Chem. A* **2022**, *126*, 9276–9302.

(73) Stropoli, S. J.; Khuu, T.; Boyer, M. A.; Karimova, N. V.; Gavin-Hanner, C. F.; Mitra, S.; Lachowicz, A. L.; Yang, N.; Gerber, R. B.; McCoy, A. B.; et al. Electronic and Mechanical Anharmonicities in the Vibrational Spectra of the H-Bonded, Cryogenically Cooled $X^- \cdot HOCl$

(X═Cl, Br, I) Complexes: Characterization of the Strong Anionic H-Bond to an Acidic OH Group. *J. Chem. Phys.* **2022**, *156*, 174303.

(74) Duschinsky, F. The Importance of the Electron Spectrum in Multi Atomic Molecules. Concerning the Franck-Condon Principle. *Acta Physicochim. USSR* **1937**, *7*, 551−566.

(75) Mok, D. K. W.; Lee, E. P. F.; Chau, F.-T.; Wang, D.; Dyke, J. M. A New Method of Calculation of Franck−Condon Factors Which Includes Allowance for Anharmonicity and the Duschinsky Effect: Simulation of the He I Photoelectron Spectrum of ClO_2. *J. Chem. Phys.* **2000**, *113*, 5791−5803.

(76) Rodriguez-Garcia, V.; Yagi, K.; Hirao, K.; Iwata, S.; Hirata, S. Franck-Condon Factors Based on Anharmonic Vibrational Wave Functions of Polyatomic Molecules. *J. Chem. Phys.* **2006**, *125*, 014109.

(77) These values are obtained directly from the VPT2 calculations, not including the frequency shifts described in Section S1.1.

(78) Weaver, A.; Arnold, D. W.; Bradforth, S. E.; Neumark, D. M. Examination of the $^2A_2{'}$ and $^2E{''}$ States of NO_3 by Ultraviolet Photoelectron-Spectroscopy of NO_3^-. *J. Chem. Phys.* **1991**, *94*, 1740−1751.

(79) Baskakov, O. I.; Markov, I. A.; Alekseev, E. A.; Motiyenko, R. A.; Lohilahti, J.; Horneman, V.-M.; Winnewisser, B. P.; Medvedev, I. R.; Lucia, F. C. D. Simultaneous Analysis of Rovibrational and Rotational Data for the 4^1, 5^1, 6^1, 7^2, 8^1, 7^19^1 and 9^2 States of HCOOH. *J. Mol. Struct.* **2006**, *795*, 54−77.

(80) Demaison, J.; Herman, M.; Liévin, J. Anharmonic Force Field of *Cis*- and *Trans*-Formic Acid from High-Level *Ab Initio* Calculations, and Analysis of Resonance Polyads. *J. Chem. Phys.* **2007**, *126*, 164305.

(81) Felker, P. M.; Zewail, A. H. Dynamics of Intramolecular Vibrational-Energy Redistribution (IVR). II. Excess Energy Dependence. *J. Chem. Phys.* **1985**, *82*, 2975−2993.

(82) Kulp, T. J.; Kim, H. L.; McDonald, J. D. Rotational Effects on Intramolecular Vibrational Relaxation in Dimethyl Ether and 1,4 Dioxane. *J. Chem. Phys.* **1986**, *85*, 211−220.

(83) Kim, H. L.; Kulp, T. J.; McDonald, J. D. Infrared Fluorescence Study on the Threshold of Intramolecular Vibrational-State Mixing. *J. Chem. Phys.* **1987**, *87*, 4376−4382.

(84) DeVine, J. A.; Weichman, M. L.; Laws, B.; Chang, J.; Babin, M. C.; Balerdi, G.; Xie, C. J.; Malbon, C. L.; Lineberger, W. C.; Yarkony, D. R.; et al. Encoding of Vinylidene Isomerization in Its Anion Photoelectron Spectrum. *Science* **2017**, *358*, 336−339.

📖 Recommended by ACS